Journal of Solid State Chemistry 183 (2010) 1278–1289

Contents lists available at ScienceDirect

Journal of Solid State Chemistry

journal homepage: www.elsevier.com/locate/jssc

X-ray structural study of intermetallic alloys RT_2Si and $RTSi_2$ (R=rare earth, T=noble metal)

Alexander Gribanov [a,b,*], Andriy Grytsiv [a], Peter Rogl [a], Yurii Seropegin [b], Gerald Giester [c]

[a] Institute of Physical Chemistry, University of Vienna, Währingerstrasse 42, A-1090 Wien, Austria
[b] Chemistry Department of the Moscow State University, Leninskie Gory, GSP-1, 119991 Moscow, Russia
[c] Institute of Mineralogy and Crystallography, University of Vienna, Althanstrasse 14, A-1090 Wien, Austria

ARTICLE INFO

Article history:
Received 30 November 2009
Received in revised form
17 March 2010
Accepted 27 March 2010
Available online 2 April 2010

Keywords:
Ternary silicides $RTSi_2$
RT_2Si
Single crystal X-ray diffraction
Powder X-ray diffraction

ABSTRACT

Two series of intermetallic alloys, RT_2Si and $RTSi_2$, have been synthesized from stoichiometric compositions. The crystal structures of $EuPt_{1+x}Si_{2-x}$ ($CeNiSi_2$-type), $CeIr_2Si$ (new structure type), $YbPd_2Si$ and $YbPt_2Si$ (both YPd_2Si-type) have been elucidated from X-ray single crystal CCD data, which were confirmed by XPD experiments. The crystal structures of $LaRh_2Si$ and $LaIr_2Si$ ($CeIr_2Si$-type), {La,Ce,Pr,Nd}$AgSi_2$ (all $TbFeSi_2$-type), and $EuPt_2Si$ (inverse $CeNiSi_2$-type) were characterized by XPD data. $RT_2Si/RTSi_2$ compounds were neither detected in as-cast alloys $Sc_{25}Pt_{50}Si_{25}$, $Eu_{25}Os_{25}Si_{50}$ and $Eu_{25}Rh_{25}Si_{50}$ nor after annealing at 900 °C. Instead, X-ray single crystal data prompted $Eu_2Os_3Si_5$ ($Sc_2Fe_3Si_5$-type) and $EuRh_{2+x}Si_{2-x}$ (x=0.04, $ThCr_2Si_2$-type) as well as a new structure type for $Sc_2Pt_3Si_2$ (own type).

1. Introduction

The discovery of heavy fermion superconductivity in compounds with non-centrosymmetric crystal structures particularly in $CePt_3Si$ [1], $CeRhSi_3$ [2] and $CeIrSi_3$ [3] has spurred increased interest also for the alloy series with stoichiometries RT_2Si and $RTSi_2$. A variety of interesting properties arise from the competition between the RKKY and Kondo interactions of the localized 4*f* electrons with conducting electrons at the Fermi-level. Hitherto known examples are as follows: $CePd_2Si$ [4], $CePt_2Si$ [5], a heavy fermion ground state in $CeRh_2Si$ [6], a Kondo-lattice exhibiting magnetic order below 2.1 K in $YbPd_2Si$ [7], heavy-fermion behavior for $CePtSi_2$ [8], valence fluctuations in $CeRhSi_2$ and $CeIrSi_2$ [9], heavy-fermion ferromagnetism in $CeRuSi_2$ [10], nonmagnetic valence fluctuations in $CeNiSi_2$ [11] and a spin-glass-like magnetic behavior in $CePdSi_2$ [12,13].

For RT_2Si and $RTSi_2$ compounds a variety of structure types are known: orthorhombic $CeNiSi_2$-type (space group *Cmcm*) [14] and its derivative $TbFeSi_2$-type (space group *Cmcm*) [15,16], orthorhombic $YIrGe_2$-type (space group *Immm*) [17], monoclinic $NdRuSi_2$-type (space group $P2_1/m$) [18,19], tetragonal $HfCuSi_2$-type (space group *P4/nmm*) [20] and the $TiMnSi_2$-type (space group *Pbam*) [21]. When T-atoms and silicon atoms exchange their sites in $CeNiSi_2$ a site exchange variant is obtained resulting in a formula RT_2Si. Hitherto known RT_2Si compounds crystallize either in the inverse $CeNiSi_2$-type or in the YPd_2Si-type (ordered Fe_3C-type, space group *Pnma*) [22].

Despite of the large volume of experimental data in the literature for intermetallics RT_2X and RTX_2, the role of transitional metals and of components X in the formation of ground states and crystal structures is not fully understood. Table 1 summarizes data on crystal structures and physical properties of the hitherto known compounds of these series. The present work is a continuation of our recent investigations of the RT_2Si series (reported in [5,7]) and extends to the search for new RT_2Si and $RTSi_2$ compounds particularly in the alloys $Eu_{25}Pt_{50}Si_{25}$, $Eu_{25}Pt_{25}Si_{50}$, $La_{25}Rh_{50}Si_{25}$, $La_{25}Ir_{50}Si_{25}$, $Ce_{25}Ir_{50}Si_{25}$, $La_{25}Ag_{25}Si_{50}$, $Ce_{25}Ag_{25}Si_{50}$, $Pr_{25}Ag_{25}Si_{50}$, $Nd_{25}Ag_{25}Si_{50}$, $Yb_{25}Pd_{50}Si_{25}$, $Yb_{25}Pt_{50}Si_{25}$, $Sc_{25}Pt_{50}Si_{25}$, $Eu_{25}Os_{25}Si_{50}$, $Eu_{25}Rh_{25}Si_{50}$ (at%) with the aim to elucidate their crystal structures.

2. Experimental techniques

Alloys of 1 g each were synthesized by standard arc-melting from high-purity elements (>99.9 mass%) on a water-cooled copper crucible in an argon environment starting from nominal compositions 1:2:1 or 1:1:2. To ensure complete fusion, all alloys were re-melted three times. Eu- and Yb-containing alloys were prepared with excess of 1 and 3 mass% of the rare-earth element to compensate losses in evaporation. The as-cast alloys were vacuum-sealed in quartz tubes and annealed at temperatures in

* Corresponding author at: Chemistry Department of the Moscow State University, Leninskie Gory, GSP-1, 119991 Moscow, Russia.
E-mail addresses: avgri@mail.ru, grav@general.chem.msu.ru (A. Gribanov).

0022-4596/$ - see front matter © 2010 Elsevier Inc. All rights reserved.
doi:10.1016/j.jssc.2010.03.038

the range 800–1050 °C for 7–20 days before being quenched in cold water. X-ray powder diffraction (XPD) patterns were collected employing a Guinier–Huber image plate system with Cu$K\alpha_1$ radiation ($\lambda=0.15406$ nm) ($8^\circ<2\theta<100^\circ$) with Ge as internal standard ($a_{Ge}=0.56579$ nm). Lattice parameters were derived using program STOE-WinXpow [23]. Quantitative X-ray Rietveld refinements were performed with the FULLPROF program [24,25], employing internal tables for X-ray atomic form factors. For several intermetallics ($CeIr_2Si$, $EuPtSi_2$, $YbPt_2Si$, $YbPd_2Si$, $Eu_2Os_3Si_5$, $Sc_2Pt_3Si_2$ and $EuRh_2Si_2$) single crystals were isolated from mechanically crushed alloys and were pre-selected on an AXS-GADDS texture goniometer. Unit cell dimensions and Laue symmetry of the structures were determined prior to X-ray intensity data collection on a four-circle Nonius Kappa diffractometer equipped with a CCD area detector and employing graphite monochromated Mo$K\alpha$ radiation ($K\alpha_1+K\alpha_2$, $\lambda=0.071073$ nm). Orientation matrix and unit cell parameters were derived using program DENZO [26]. No absorption corrections were made because of the rather regular crystal shape and small dimensions of the investigated specimens. The structures were solved by direct methods and refined with the SHELXL-97 program [27]. Atom parameters were standardized using program *Structure Tidy* [28].

3. Results and discussion

In the present investigation crystal structures have been determined for 11 ternary compounds with stoichiometry RT_2Si or $RTSi_2$, namely: $EuPt_2Si$, $EuPtSi_2$, $LaRh_2Si$, $LaIr_2Si$, $CeIr_2Si$, $LaAgSi_2$, $CeAgSi_2$, $PrAgSi_2$, $NdAgSi_2$, $YbPd_2Si$, $YbPt_2Si$. In the alloys $Sc_{25}Pt_{50}Si_{25}$, $Eu_{25}Os_{25}Si_{50}$, $Eu_{25}Rh_{25}Si_{50}$ no corresponding RT_2Si or $RTSi_2$ phases were detected. Nevertheless the crystal structures of novel compounds $Sc_2Pt_3Si_2$ and $Eu_2Os_3Si_5$, as well as of $EuRh_2Si_2$ (structure known before from powder data [29–31]) were determined on the basis of single crystal data.

fTable 1
Literature data of crystal structures and physical properties for selected compounds RT_2Si and $RTSi_2$.

Compound	Structure type (space group)	a (nm)	b (nm)	c (nm)	Ref.	Physical property	Ref.
$CeRh_2Si$	$CeNiSi_2$-inverse (*Cmcm*)	0.40413	1.7730	0.40675	[32]	CW ($\mu_{eff}=2.46\mu_B$, $\Theta_p=-70$ K), T_{sg}~1 K	[6]
$CeRh_{1.88}Si_{1.12}$	$CeNiSi_2$-inverse (*Cmcm*)	0.40591	1.7673	0.40736	[33]		
$CeRh_{2-x}Si_{1+x}$	$CeIr_2Si$ ($I4_1/amd$)	0.40521		3.5556	$x=0$ [33]		
$0.0\le x\le 0.1$[33]		0.40560		3.5472	$x=0.1$[33]		
$YbPd_2Si$	–	–	–	–	[43]	Kondo-compound	[43]
	YPd_2Si (*Pnma*)	7.1775	6.9335	5.4406	[7]	CW ($\mu_{eff}=4.39\mu_B$, $\Theta_p=-19.5$ K), $T_{magn}=2.1$ K	[7]
$LaPt_2Si$	$CeNiSi_2$- inverse (*Cmcm*)	0.41721	1.7894	0.42378	[5]	$\gamma=5.5$ mJ/mol K^2, $\Theta_D=225$ K	[5]
$CePt_2Si$	$CeNiSi_2$- inverse (*Cmcm*)	0.40987	1.8032	0.41677	[5]	CW ($\mu_{eff}=2.32\mu_B$, $\Theta_p=-47$ K), $T_{magn1}=6.6$ K, $T_{magn2}=5.6$ K	[5]
$LaRhSi_2$	$CeNiSi_2$ (*Cmcm*)	–	–	–	[44]	SC, $T_c=3.42$	[44]
$CeRhSi_2$	$CeNiSi_2$ (*Cmcm*)	–	–	–	[44]		
		0.42661	1.6758	0.41708	[9]	MV, $T_{sf}=134$	[9,45]
		0.4289	1.6805	0.4232	[45]	MV	[45]
		0.4310	1.674	0.421	[46]	$Ce^{+3.07}$	[46]
$CeRh_{1-x}Si_{2+x}$		0.42629	1.67456	0.41731	$x=0$ [33]		
$0\le x\le 0.32$		0.42582	1.67526	0.41773	$x=0.15$ [33]		
		0.42566(4)	1.6768(2)	0.41763(4)	$x_{max}=0.32$ [33]		
$CePtSi_2$	$CeNiSi_2$ (*Cmcm*)	0.4288	1.6718	0.4238	[8]	CW ($\mu_{eff}=2.56\mu_B$, $\Theta_p=-17$ K), HF, $\gamma=1700$ mJ/mol K^2 at 1.25 K	[8]
		0.4288	1.6862	0.4248	[47]	$\gamma=395.1$ mJ/mol K^2	[47]
		0.428	1.686	0.424	[46]	AF, T_N~1.5 K	[46]
$CeIrSi_2$	$CeNiSi_2$ (*Cmcm*)	0.42580	1.6754	0.41917	[9]	MV, $T_{sf}=249$	[9]
		0.4297	1.6754	0.4190	[12]	MV	[12]
		0.4274	1.6745	0.4182	[47]	MV	[47]
$LaIrSi_2$	$CeNiSi_2$ (*Cmcm*)	–	–	–	[44]	SC, $T_c=2.03$	[44]
		4.323	16.841	4.227	[12]		
$CeAgSi_2$	Unknown	–	–	–	[38]		

CW—Curie–Weiss behavior; μ_{ef}—effective magnetic moment; Θ_p—paramagnetic Curie temperature; Θ_D—Debye temperature; T_{sg}—spin-glass transition; γ—Sommerfeld coefficient; SC—superconductivity; T_c—temperature of the superconductivity transition; T_{magn}—temperature of the magnetic transition; MV—mixed valence; T_{sf}—spin fluctuation temperature; AF—antiferromagnetic ordering; T_N—Neel temperature; HF—heavy fermion behavior.

Table 2.
Unit cell dimensions from XPD data for the compounds with the $CeNiSi_2$-type and related derivatives: $LaRh_2Si$, {La,Ce}Ir_2Si, $EuPt_2Si$, $EuPtSi_2$, {La,Ce,Pr,Nd}$AgSi_2$.

Compound	Prototype (space group)	a (nm)	b (nm)	c (nm)	V (nm)
$LaRh_2Si$	$CeIr_2Si$ ($I4_1/amd$)	0.41018(9)		3.552(1)	0.5976(4)
$CeIr_2Si$	$CeIr_2Si$ ($I4_1/amd$)	0.40680(4)		3.5399(4)	0.5858(1)
$CeIr_{2-x}Si_{1+x}$	$CeNiSi_2$-inv. (*Cmcm*)	0.40680(4)	1.7648(1)	0.40658(4)	0.29190(5)
In the sample $Ce_{25}Ir_{48}Si_{27}$ (at%)					
$LaIr_2Si$	$CeIr_2Si$ ($I4_1/amd$)	0.41284(2)		3.5297(2)	0.60160(6)
$EuPt_2Si$	$CeNiSi_2$-inv. (*Cmcm*)	0.41580(5)	1.7793(3)	0.41704(6)	0.30854(5)
$EuPt_{1+x}Si_{2-x}$ ($x=0$)	$CeNiSi_2$ (*Cmcm*)	0.43522(3)	1.69787(11)	0.41513(3)	0.30676(3)
$LaAgSi_2$	$TbFeSi_2$ (*Cmcm*)	0.43160(7)	1.7533(3)	0.42742(6)	0.3235(1)
$CeAgSi_2$	$TbFeSi_2$ (*Cmcm*)	0.42528(2)	1.75492(8)	0.42326(2)	0.31589(4)
$PrAgSi_2$	$TbFeSi_2$ (*Cmcm*)	0.42244(7)	1.7522(4)	0.42164(10)	0.3121(1)
$NdAgSi_2$	$TbFeSi_2$ (*Cmcm*)	0.41991(4)	1.7498(2)	0.42015(4)	0.30871(5)

Table 3
X-ray crystallographic data and structure refinement for $EuPt_{1+x}Si_{2-x}$ ($x=0.075$), $CeIr_2Si$ and $CeAgSi_2$ standardized with program *Structure Tidy* [28].

Parameter	$EuPt_{1+x}Si_{2-x}$	$CeIr_2Si$	$CeAgSi_2$
Alloy composition (at%)	$Eu_{25}Pt_{25}Si_{50}$	$Ce_{25}Ir_{50}Si_{25}$	$Ce_{25}Ag_{25}Si_{50}$
Crystal size (μm)	$50\times50\times50$	$30\times30\times30$	powder
Space group	*Cmcm*, origin at inv. Centre	$I4_1/amd$, origin at inv. centre	*Cmcm*, origin at inv. centre
Prototype	$CeNiSi_2$	$CeIr_2Si$	$TbFeSi_2$
Pearson symbol	*o*C16	tI32	oC16
Lattice parameters (nm)[a]	$a=0.43567(2)$ $b=1.69899(9)$ $c=0.41517(2)$	$a=0.40698(1)$ $c=3.54085(10)$	a=0.42531(4) b=1.7551(2) c=0.42331(4)
Cell volume (nm^3)	0.30731(3)	0.58648(3)	0.31598(7)
Chemical formula	$EuPt_{1.075}Si_{1.925}$	$CeIr_2Si$	$CeAgSi_2$
Formula weight, *M*	415.75	552.61	304.17
Number of formula units in unit cell, *Z*	4	8	4
Calculated density (g/cm^3)	8.986	12.517	6.39
Absorption coefficient, μ_{abs} (mm^{-1})	69.516	105.865	
2θ range up to (°)	72.48	72.37	$8\le2\Theta\le100$
Reflections in refinement	$406\ge4\sigma(F_o)$ of 444	$351\ge4\sigma(F_o)$ of 436	124 reflections
Index range	$-7\le h\le7$ $-27\le k\le28$ $-6\le l\le\ \le6$	$-6\le h\le6$ $-4\le k\le4$ $-57\le l\le56$	
Number of variables	20	16	30
$R=\Sigma\|\|F_0\|-\|F_c\|\|/\Sigma\|F_0\|$	0.028	0.034	$R_F=0.047$, $R_B=0.080$
R_{Int}	0.018	0.030	$R_e=0.022$
wR_2	0.061	0.108	$R_{wP}=0.079$
Goodness of fit, $S=\{\Sigma[w(F_o^2-F_c^2)^2]/(n-p)\}^{1/2}$	1.196	1.903	$\chi^2=13.0$
Extinction (Zachariasen)	0.0009(2)	0.0011(1)	
Atom parameters			
Atom site 1	**4 Eu1** in 4*c* (0,*y*, 1/4); $y=0.39435(3)$	**8 Ce1** in 8*e* (0,1/4,*z*); $z=0.19951(2)$	**4 Ce1** in 4*c* (0,*y*,1/4) $y=0.40204(3)$
Occupation $U_{eq.}$	1.00 0.0049(2)	1.00 0.0043(2)	1.00 $B_{iso}=2.43(3)$
Atom site 2	**4 Pt1** in 4*c* (0,*y*,1/4); $y=0.17969(3)$	**4 Ir1** in 4*a* (0,3/4,1/8);	**4 Ag1** in 4*c* (0,*y*,1/4) $y=0.74844(4)$
Occupation $U_{eq.}$	1.00 0.0072(2)	1.00 0.0017(2)	1.00 $B_{iso}=1.95(9)$
Atom site 3	**4 Si1** in 4*c* (0,*y*,1/4); $y=0.7481(2)$	**4 Ir2** in 4*b* (0,1/4,3/8);	**4 Si1** in 4*c* (0,*y*,1/4) $y=0.0334(2)$
Occupation $U_{eq.}$	1.00 0.0055(6)	1.00 0.0017(2)	1.00 $B_{iso}=1.11(8)$
Atom site 4	**4 Si2/Pt** in 4*c* (0,*y*,1/4); $y=0.0349(2)$	**8 Ir3** in 8*e* (0,1/4,*z*); $z=0.02191(2)$	**4 Si2** in 4*c* (0,*y*,1/4) $y=0.1621(2)$
Occupation $U_{eq.}$	0.925(3) Si+0.075 Pt 0.0095(6)	1.00 0.0062(2)	1.00 $B_{iso}=1.82(3)$
Atom site 5		**8 Si1** in 8*e* (0,1/4,*z*); $z=0.0886(1)$	
Occupation $U_{eq.}$		1.00 0.0030(7)	

Residual density; e/Å^3 max; min	5.60	−3.62		7.95	−6.29			
Interatomic distances, nm (eds < 0.0003 nm)	Eu1-	2 Si1	0.3188	Ce1 -	4 Ir3	0.3051	Ce1	2 Si1	0.3137
		2 Si2	0.3232		4 Si1	0.3179		4 Si2	0.3205
		4 Si2	0.3240		2 Ir3	0.3273		4 Si1	0.3207
		4 Pt1	0.3261		2 Ir1	0.3332		2 Ag1	0.3385
		2 Si1	0.3305		2 Ir2	0.3332		2 Ag1	0.3434
	Pt1-	1 Pt1	0.3647	Ir1-	4 Si1	0.2408	Si2	1 Si1	0.2258
		2 Si1	0.2412		4 Ir2	0.2878		2 Ag1	0.2611
		1 Si2	0.2460		4 Ce1	0.3332		2 Ag1	0.2635
		2 Si1	0.2469	Ir2-	4 Si1	0.2408		4 Ce1	0.3205
	Si1-	4 Eu1	0.3261		4 Ir1	0.2878	Si1	1 Si2	0.2258
		1 Eu1	0.3647		4 Ce1	0.3332		2 Si1	0.2420
		2 Pt1	0.2412	Ir3-	1 Si1	0.2363		2 Ce1	0.3137
		2 Pt1	0.2469		2 Ir3	0.2559		4 Ce1	0.3207
		4 Si1	0.3010		4 Ce1	0.3051	Ag1	2 Si2	0.2611
	Si2-	2 Eu1	0.3188		2 Ce1	0.3273		2 Si2	0.2635
		2 Eu1	0.3305	Si1-	1 Ir3	0.2362		4 Ag1	0.3001

Table 3 (*continued*)

Parameter	$EuPt_{1+x}Si_{2-x}$		$CeIr_2Si$		$CeAgSi_2$	
	2 Si2	0.2390	2 Ir1	0.2408	2 Ce1	0.3385
	1 Pt1	0.2460	2 Ir2	0.2407	2 Ce1	0.3434
			4 Ce1	0.3179		

For Rietveld refinement of $CeAgSi_2$ (XPD experiment).

$$R_F = \sum_{hkl}|F_{hkl}(obs)-F_{hkl}(calc)|/\sum_{hkl}|F_{hkl}(obs)|$$

$$R_B = \sum_{hkl}|I_{hkl}(obs)-I_{hkl}(calc)|/\sum_{hkl}|I_{hkl}(obs)|$$

$$R_e = \left[\frac{n-p}{\sum_i w_i y_i^2}\right]^{1/2}$$

$(n–p)$ is the number of degrees of freedom, n the number of the points in the refinement, p the number of refined parameters $\chi^2 = \sum_{i=1}^{n} w_i\{y_i-y_{c,i}(\vec{\alpha})\}^2$ where $\vec{\alpha} = (\alpha_1,\alpha_2,\alpha_3,\ldots,\alpha_p)$—parameter vector.

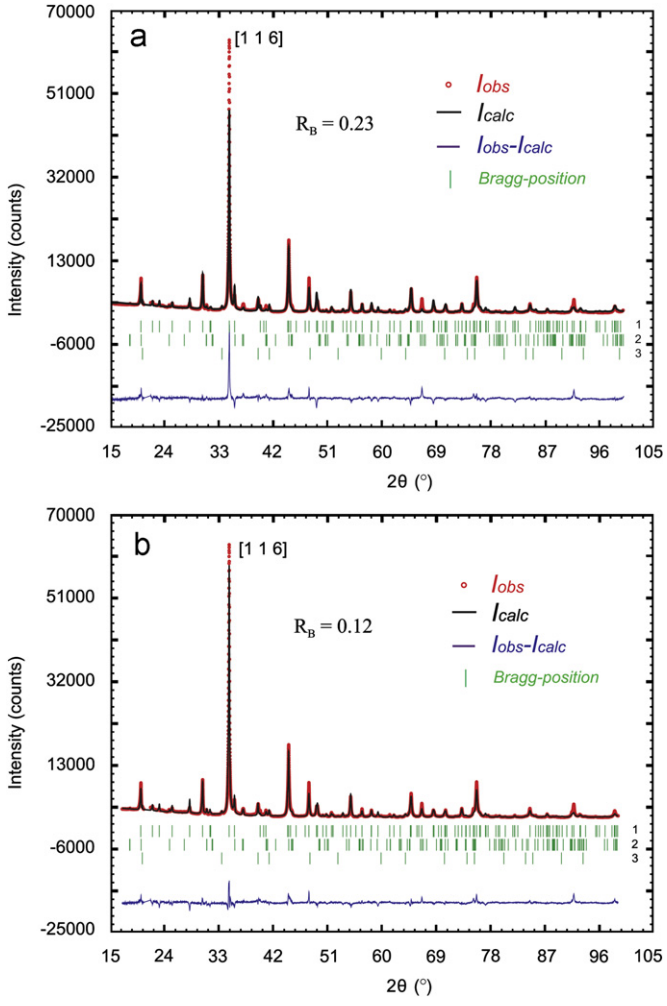

Fig. 1. Rietveld refinement of the $CeIr_2Si$ XPD pattern performed without preferred orientation calculation (a) and with preferred orientation calculation along [116] axis (b) (modified March's function was used, $P_h = G_2+(1-G_2)\{(G_1\cos\alpha_h)^2+(\sin^2\alpha_h)/G_1\}^{-3/2}$, where G_1 and G_2 are refinable parameters and α_h a acute angle between the scattering vector and the normal to the crystallites. For $CeIr_2Si$ (b) $G_1 = 0.783(3)$ and $G_2 = 0$. At the bottom of the each figure (a) and (b) the Bragg-positions 1, 2 and 3 correspond to $CeIr_2Si$ (main phase), $CeIr_3Si_2$ (small amount) and $CeIr_2$ (trace amount).

3.1. *Compounds with $CeNiSi_2$-type and related structure types*

This chapter covers compounds of the RT_2Si and $RTSi_2$ series, which crystallize in the orthorhombic $CeNiSi_2$-type or its site-exchange variants, i.e. the $TbFeSi_2$-type [15] and the $CeRh_2Si$-type [32], as well as in a new tetragonal $CeIr_2Si$-type determined in the present work for the first time. Table 2 lists structure types and lattice parameters determined from XPD experiments for $LaRh_2Si$, $CeIr_2Si$, $CeIr_{2-x}Si_{1+x}$, $LaIr_2Si$, $EuPt_2Si$, $EuPtSi_2$, $LaAgSi_2$, $CeAgSi_2$, $PrAgSi_2$ and $NdAgSi_2$. The crystal structures of $EuPtSi_2$ and $CeIr_2Si$ were derived from single crystal X-ray data and the corresponding crystallographic data are summarized in Table 3.

3.1.1. *X-ray single crystal studies of $EuPt_{1+x}Si_{2-x}$ and $CeIr_2Si$*

A single crystal from the as-cast alloy $Eu_{25}Pt_{25}Si_{50}$ (in at%), revealed orthorhombic symmetry with space group *Cmcm* and lattice parameters: $a = 0.43567(2)$ nm, $b = 1.69899(9)$ nm, $c = 0.41517(2)$ nm. The crystal structure was solved by direct methods yielding a partial random distribution of Pt and Si in one of the 4*c* sites yielding a chemical formula $EuPt1+xSi_{2-x}$ ($x = 0.075$). Results of the refinement, which converged to $R = 0.028$ with residual electron densities smaller than $\pm 5.6\,e^-/Å^3$, are summarized in Table 3. Besides the detected atom disorder $EuPt_{1+x}Si_{2-x}$ is isotypic with $CeNiSi_2$.

The X-ray intensity pattern of a suitable single crystal, taken from the alloy $Ce_{25}Ir_{50}Si_{25}$ (annealed at 850 °C) was completely indexed on a tetragonal unit cell ($a = 0.40698(1)$ nm and $c = 3.54085(10)$ nm) consistent with space group symmetry $I4_1/amd$ (No. 141). The structure was solved by direct methods and refined to $R = 0.034$ with residual electron densities smaller than $\pm 8.0\,e^-/Å^3$, yielding a completely ordered atom arrangement (see Table 3). The same type of structure was detected from the XPD patterns of $LaIr_2Si$, $CeRh_2Si$ and $LaRh_2Si$.

3.1.2. *Tetragonal and orthorhombic variants of RT_2Si compounds*

The new tetragonal $CeIr_2Si$-type has also been detected in our investigation of the Ce–Rh–Si system [33] forming at 800 °C a small homogeneous range $CeRh_{2-x}Si_{1+x}$ ($0 \le x \le 0.1$). The previously reported orthorhombic $CeRh_2Si$ compound [32] was observed in our investigation at the composition $Ce_{25}Rh_{47}Si_{28}$ with a corresponding formula $CeRh_{1.88}Si_{1.12}$. Despite the orthorhombic and tetragonal phases are very close to each other, they

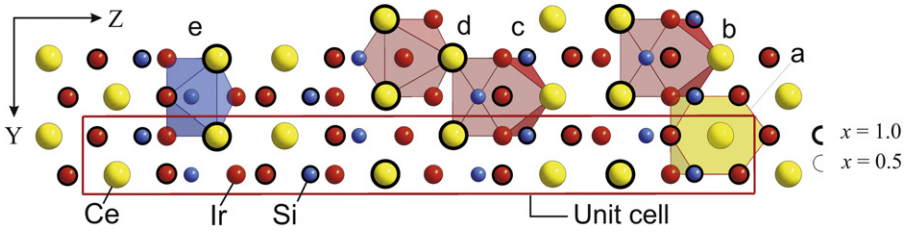

Fig. 2. Projection of the crystal structure of $CeIr_2Si$ onto the *XZ* plane; the coordination polyhedra of the sites are outlined: Ce1 (a), Ir1 (b), Ir2 (c), Ir3 (d) and Si1 (e).

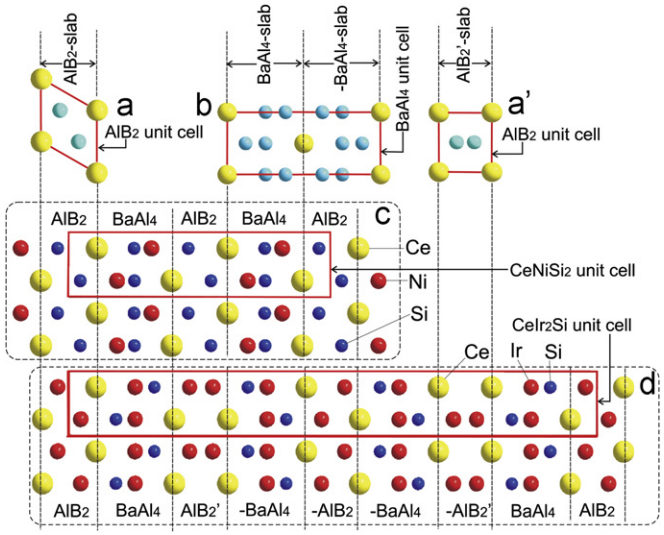

Fig. 3. Structure types of orthorhombic $CeNiSi_2$ and tetragonal $CeIr_2Si$ shown as a packing of slabs of AlB_2 and $BaAl_4$ type. $|AlB_2|$ and $|AlB_2'|$ reflect different views on the AlB_2 unit cell (**a** and **a**′) and corresponding slabs. The slabs $|BaAl_4|$ and $|-BaAl_4|$ indicate two halves of the $BaAl_4$ unit cell (**b**) which are related via an inversion center. Packing of slabs in the $CeNiSi_2$-type (**c**). In the $CeIr_2Si$ structure (**d**) AlB_2 and AlB_2' slabs are shifted by 1/2 ***a*** in comparison to $(-AlB_2)$ and $(-AlB_2')$ slabs.

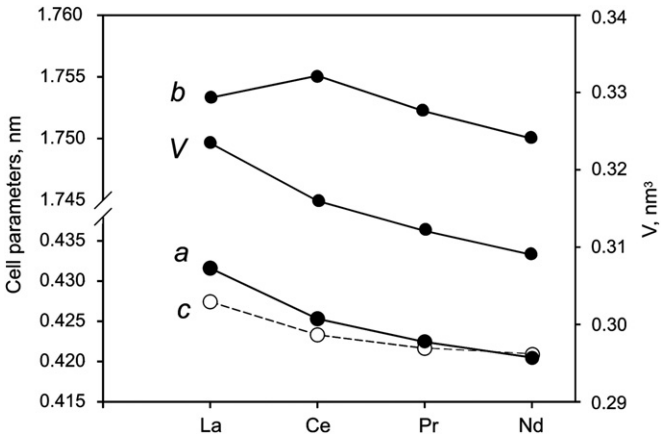

Fig. 4. Unit cell parameters of $RAgSi_2$ as a function of rare-earths.

were clearly distinguished in XPD. Whilst the tetragonal structure is observed in both the as-cast and the annealed alloy $Ce_{25}Rh_{50}Si_{25}$, orthorhombic $CeRh_{1.88}Si_{1.12}$ together with the tetragonal structure appeared in alloys with a higher content of silicon. Checking the Ce–Ir–Si system at 800 °C near composition $Ce_{25}Ir_{50}Si_{25}$ we found that besides the new tetragonal $CeIr_2Si$-type the orthorhombic $CeNiSi_2$-inverse type appeared in small amounts in both the as-cast and the alloy $Ce_{25}Ir_{48}Si_{27}$ annealed at 1050 °C. At the stoichiometric composition 1:2:1 the tetragonal

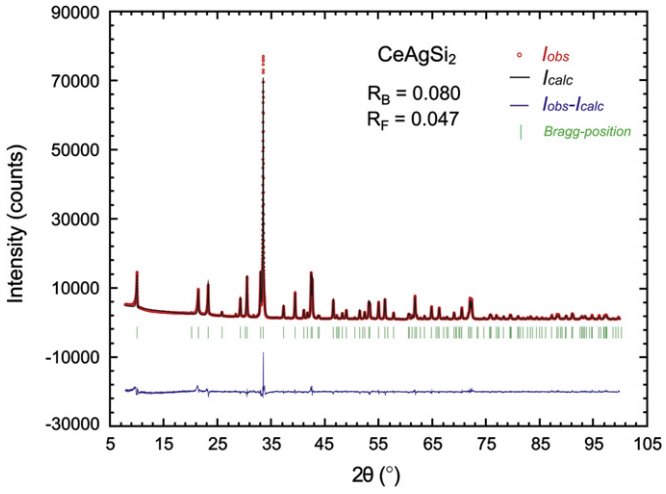

Fig. 5. Rietveld refinement of the $CeAgSi_2$.

$CeIr_2Si$-type phase is found as the main phase with a small amount of orthorhombic $CeIr_3Si_2$ and a trace of cubic $CeIr_2$. La-containing analogues $LaRh_2Si$ and $LaIr_2Si$ showed only the existence of the tetragonal structure in annealed samples $La_{25}T_{50}Si_{25}$ but no orthorhombic $CeNiSi_2$-inverse type could be discovered. A common peculiarity of all four XPD patterns of the $R_{25}T_{50}Si_{25}$ compounds ($LaIr_2Si$, $CeIr_2Si$, $LaRh_2Si$ and $CeRh_2Si$) is a small but distinct disagreement between calculated and observed intensities (Fig. 1a). Preferred orientation (direction [116]) improved the Rietveld refinement from $R_B=0.23$ to $R_B=0.12$ but could not fully remove the discrepancies (Fig. 1b). Attempts to overcome preferred orientation in X-ray sample preparation using a powder-mixture with starch, special glass powder or a special powder support with sticky surface were unsuccessful.

To ensure the result of the crystal structure determination, a second single crystal from an independently prepared $CeIr_2Si$ alloy was investigated but resulted in an identical set of atom parameters. Similarly, a Rietveld powder refinement of a mix of the two closely related crystal structures did not remove the disagreements in the powder intensities. In a recently published work of Muro et al. [6] on the $CeRh_2Si$ phase, the authors confirmed from powder X-ray diffraction the presence of a main phase with inverse $CeNiSi_2$ structure besides some amount of secondary $CeRh_3Si_2$. Electron probe microanalysis measurements indicated a homogeneity region of about 5 at% assuming random Si/Rh replacement. A tetragonal structure was not detected.

3.1.3. *Crystal chemistry of $CeIr_2Si$*

Fig. 2 shows the crystal structure of $CeIr_2Si$ as a projection on the *YZ* plane and outlines the coordination polyhedra for all atom sites. Cerium atoms (Fig. 2a) are located in hexagonal prisms with two additional atoms (CN=14). Both Ir1 and Ir2 atoms have identical coordination polyhedra (Fig. 2b and c): each of these

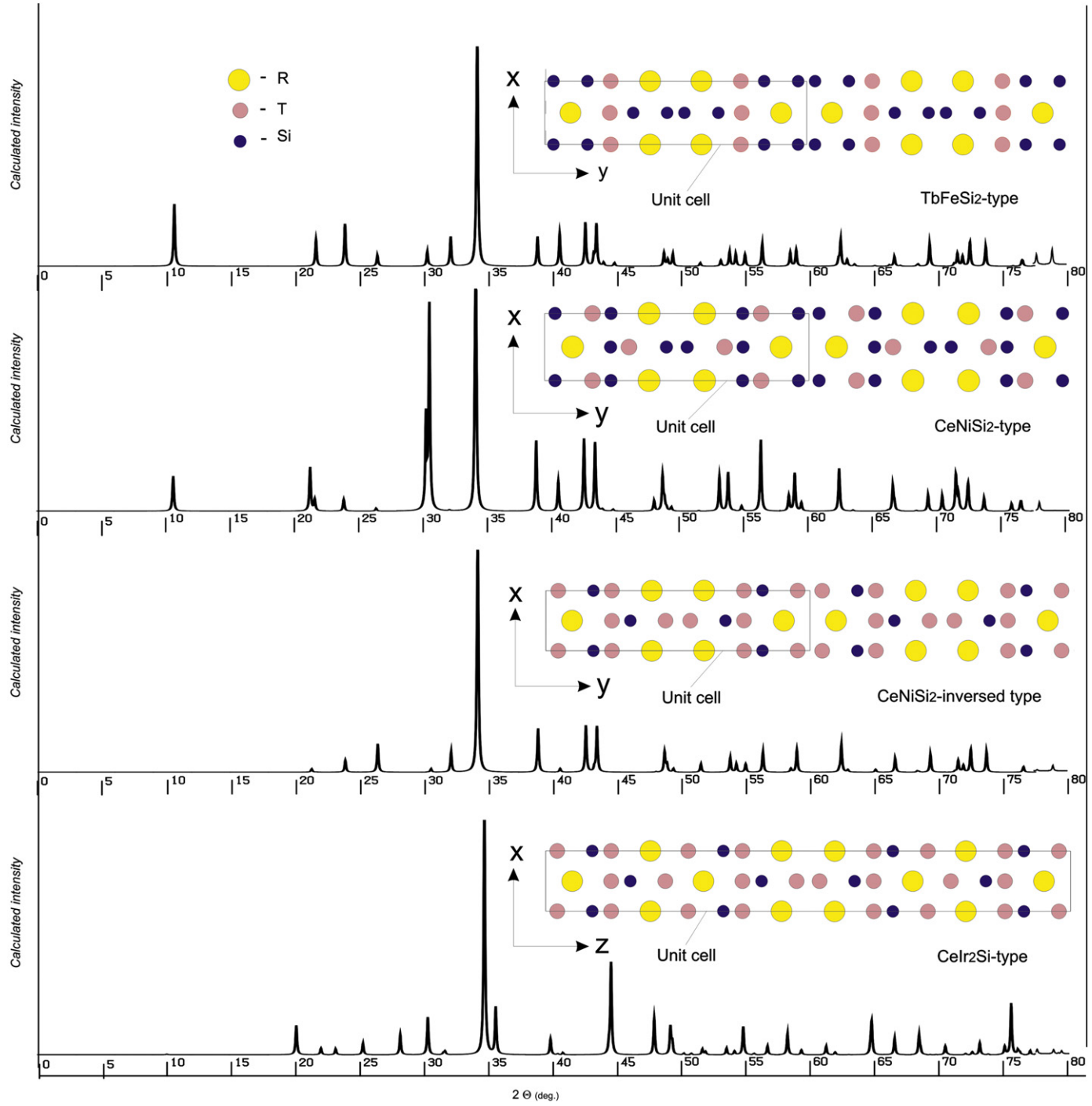

Fig. 6. Comparison of the structure types of $TbFeSi_2$, $CeNiSi_2$, $CeNiSi_2$-inverse and $CeIr_2Si$. Simulated powder diffraction patterns of the hypothetical compounds constructed from Ce, Rh and Si atoms; unit cells with identical dimensions.

atoms is surrounded by four cerium atoms, four iridium atoms and four silicon atoms, which form a quadrangular prism with four additional apexes (CN=12). Ir3 atoms center triangular prisms with three additional atoms (CN=9; Fig. 2d). The coordination polyhedron of the Si atom is a quadrangular antiprism with one additional atom (CN=9, Fig. 2e).

The interrelation between orthorhombic $CeNiSi_2$ and tetragonal $CeIr_2Si$ can be conceived from Fig. 3, where they are presented as a packing of slabs cut from AlB_2- and $BaAl_4$-types. The interatomic distances in the $CeIr_2Si$ crystal structure reflect the sum of metal radii (Table 3).

3.1.4. *Formation and crystal structure of {La,Ce,Pr,Nd}$AgSi_2$*

Although $RAgSi_2$ phases were not reported in previous phase diagram work concerning the ternary systems Nd–Ag–Si at 600 °C [34], Ce–Ag–Si at 500 °C [35,36] and Pr–Ag–Si at 500 and 800 °C [37], a compound $CeAgSi_2$ was detected by Cordruwisch et al. [38] after annealing at 850 °C for 330 h. The crystal structure of it was not determined. In the present work we established the crystal structure of $RAgSi_2$ (R=La, Ce, Pr, Nd) to belong to the $TbFeSi_2$-type. For our preparation of $RAgSi_2$ samples different temperatures and annealing times were applied. A single-phase sample of $CeAgSi_2$ was obtained after 30 days exposure at 900 °C followed

Table 4
X-ray crystallographic data and structure refinement for $YbPd_2Si$ and $YbPt_2Si$ standardized with program *Structure Tidy* [28].

Parameter	$YbPd_2Si$			$YbPt_2Si$		
Alloy composition (at%)	$Yb_{25}Pd_{50}Si_{25}$			$Yb_{25}Pt_{50}Si_{25}$		
Crystal size (μm)	$50\times50\times50$			$50\times50\times50$		
Space group	*Pnma*			Pnma		
	origin at inv. centre			Origin at inv. centre		
Prototype	YPd_2Si (ordered Fe_3C)			YPd_2Si (ordered Fe_3C)		
Pearson symbol	*oP*16			oP16		
Lattice parameters (nm)[a]	$a=0.71775(2)$			a=0.71841(2)		
	$b=0.69335(2)$			b=0.69151(2)		
	$c=0.54406(2)$			c=0.54098(2)		
Cell volume (nm^3)	0.27075(2)			0.26875(2)		
Chemical formula	$YbPd_2Si$			$YbPt_2Si$		
Formula weight, *M*	413.93			591.31		
Number of formula units in unit cell, *Z*	4			4		
Calculated density (g/cm^3)	10.155			14.614		
Absorption coefficient, μ_{abs} (mm^{-1})	47.468			138.432		
2θ range up to (°)	72.54			72.48		
Reflections in refinement	$639 \leqslant 4\sigma(F_o)$ of 688			$628 \leqslant 4\sigma(F_o)$ of 679		
Index range	$-11\leqslant h\leqslant11$			$-11\leqslant h\leqslant11$		
	$-11\leqslant k\leqslant11$			$-11\leqslant k\leqslant11$		
	$-8\leqslant l\leqslant8$			$-8\leqslant l\leqslant8$		
Number of variables	23			23		
$R=\Sigma\|\|F_o\|-\|F_c\|\|/\Sigma\|F_o\|$	0.019			0.025		
R_{Int}	0.019			0.025		
wR_2	0.046			0.065		
Goodness of fit, $S=\{\Sigma[w(F_o^2-F_c^2)^2]/(n-p)\}^{1/2}$	1.077			1.092		
Extinction (Zachariasen)	0.0016(3)			0.0018(2)		
Atom parameters						
Atom site 1	**4 Yb1** in 4*c* (*x*,1/4,*z*);			**4 Yb1** in 4*c* (*x*,1/4,*z*);		
	$x=0.02662(3)$			$x=0.02570(6)$		
	$z=0.63990(4)$			$z=0.63381(8)$		
Occupation	1.00			1.00		
$U_{eq.}$	0.00771(8)			0.0050(1)		
Atom site 2	**8 Pd1** in 8*d* (*x*,*y*,*z*);			**8 Pt1** in 8*d* (*x*,*y*,*z*);		
	$x=0.17897(4)$			$x=0.18212(4)$		
	$y=0.05161(4)$			$y=0.05092(4)$		
	$z=0.09370(5)$			$z=0.09147(5)$		
Occupation	1.00			1.00		
$U_{eq.}$	0.00774(8)			0.0051(1)		
Atom site 3	**4 Si1** in 4*c* (*x*,1/4,*z*);			**4 Si1** in 4*c* (*x*,1/4,*z*);		
	$x=0.3779(2)$			$x=0.3801(4)$		
	$z=0.3594(3)$			$z=0.3655(5)$		
Occupation	1.00			1.00		
$U_{eq.}$	0.0071(2)			0.0050(5)		
Residual density; e/Å^3 max; min		1.83	−2.70		5.58	−4.36
Interatomic distances, nm, (eds < 0.0003 nm)	Yb1-	1 Si1	0.2919	Yb1-	1 Si1	0.2897
		1 Si1	0.2926		1 Si1	0.2904
		2 Pd1	0.2941		1 Si1	0.2931
		1 Si1	0.2947		2 Pt1	0.2961
		2 Pd1	0.2984		2 Pt1	0.2965
		2 Pd1	0.3031		2 Pt1	0.3048
		2 Pd1	0.3120		2 Pt1	0.3078
		2 Pd1	0.3452		2 Pt1	0.3430
	Pd1-	1 Si1	0.2454	Pt1-	1 Si1	0.2455
		1 Si1	0.2483		1 Si1	0.2473
		1 Si1	0.2575		1 Si1	0.2580
		1 Pd1	0.2751		1 Pt1	0.2753
		1 Pd1	0.2855		1 Pt1	0.2885
		1 Yb1	0.2941		2 Pt1	0.2960
		1 Yb1	0.2984		1 Yb1	0.2961
		2 Pd1	0.2992		1 Yb1	0.2965
		1 Yb1	0.3031		1 Yb1	0.3048
		1 Yb1	0.3120		1 Yb1	0.3078
		1 Yb1	0.3452		1 Yb1	0.3430
	Si1-	2 Pd1	0.2454	Si1-	2 Pt1	0.2455
		2 Pd1	0.2483		2 Pt1	0.2473
		2 Pd1	0.2575		2 Pt1	0.2580
		1 Yb1	0.2919		1 Yb1	0.2897
		1 Yb1	0.2926		1 Yb1	0.2904
		1 Yb1	0.2947		1 Yb1	0.2931

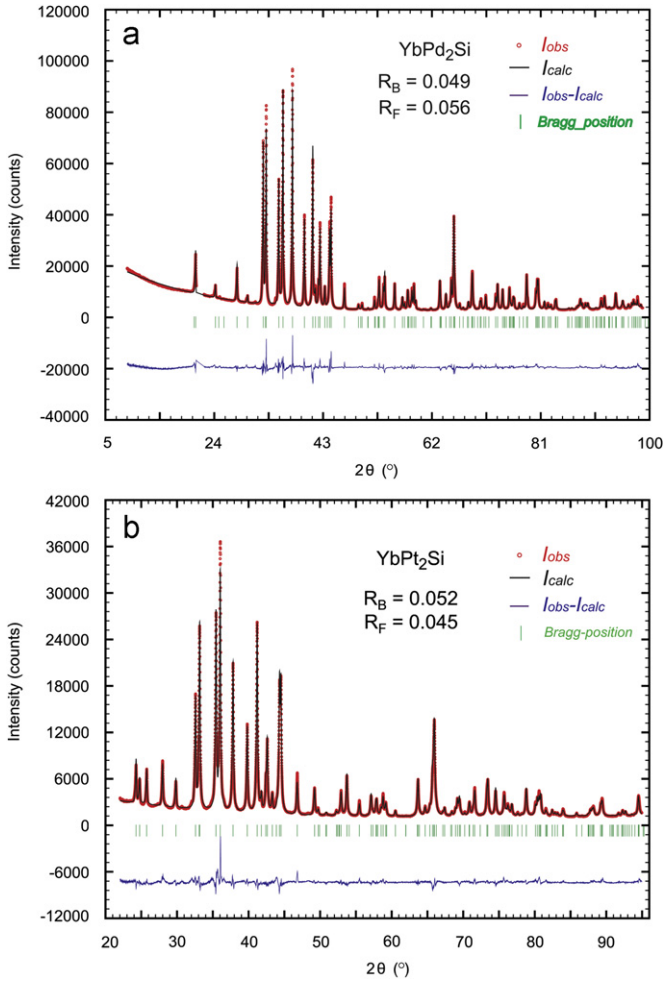

Fig. 7. Rietveld refinements for $YbPd_2Si$ (a) and $YbPt_2Si$ (b).

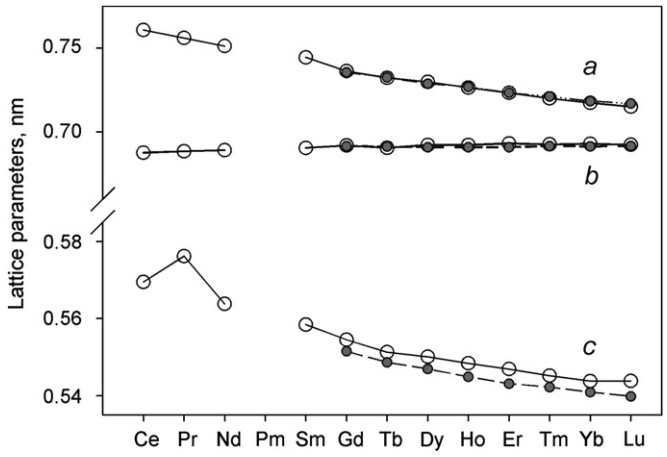

Fig. 8. Rare-earth elements versus unit cell parameters *a*, *b* and *c* for compounds RPd_2Si (open circles) and RPt_2Si (filled circles) with the YPd_2Si type structure. The new values of $YbPd_2Si$ and $YbPt_2Si$ have been added to the $R(Pd,Pt)_2Si$ data [22].

by 28 days at 850 °C. La- and Pr-containing alloys were annealed at 850 °C (30 days), 950 °C (30 days) and 1050 °C (6 days). For the latter two alloys the higher temperature resulted in a higher content of the $RAgSi_2$ phase. The Nd-containing alloy revealed a complex microstructure: both as-cast and annealed samples besides $NdAgSi_2$ contained significant amounts of $Nd(Ag,Si)_2$ with the $ThSi_2$-type structure and unknown phase(s). The highest content of the $NdAgSi_2$ phase was observed after annealing at 850 °C (25 days). La- and Pr-containing compounds were obtained as the main phases in non-single phase samples. Nevertheless unit cell parameters were easily derived for $LaAgSi_2$, $PrAgSi_2$ and $NdAgSi_2$ (see Table 2). In all cases $RAgSi_2$ (also for short-term anneal in $CeAgSi_2$) the tetragonal solid solution phase based on binary RSi_2 was detected by XPD. Fig. 4 illustrates the unit cell parameters of $RAgSi_2$ versus rare-earths *R* reflecting the lanthanoid contraction from La to Nd. Unexpected behavior is observed for the *b* parameter in the La-containing compound but this effect is overlapped by increased *a* and *c* values, so that the cell volume of $LaAgSi_2$ closely follows the expected trend (Fig. 4). Crystal data from Rietveld refinement for $CeAgSi_2$ (see Fig. 5) are summarized in Table 3. $CeAgSi_2$ shows full atom order with all crystallographic sites fully occupied. Our results for $CeAgSi_2$ are similar to those for $TbFeSi_2$ reported as a fully ordered packing of atoms [15], in contrast to the data of [16] who observed a half occupation of transitional metals site from single crystal X-ray data for $TbFe_{0.52}Si_2$, $HoFe_{0.5}Si_2$ and $DyFe_{0.5}Si_2$.

3.1.5. Crystal chemistry of $CeNiSi_2$ and related types

In the orthorhombic $CeNiSi_2$-type with space group *Cmcm* four crystallographic sites 4*c* (0,*y*,1/4) are occupied with different *y*: $y_1 \sim 0.40$, $y_2 \sim 0.16$, $y_3 \sim 0.04$ and $y_4 \sim 0.75$. Ce atoms in prototype $CeNiSi_2$ are in the position with $y_1 \sim 0.40$, T atoms (Ni) in position with y_2, while the silicon atoms occupy two sites with y_3 and y_4 arriving at a completely ordered structure. In the structures of $CeRh_2Si$ (as published in [32]) and $TbFeSi_2$ [15] rare-earth atoms are located in the position with $y_1 \sim 0.40$, as a common rare-earth site for the all three structure types. In $CeRh_2Si$ (inverse structure) one can observe a site exchange: T atoms (Rh) are located in the former Si positions (in the sites with y_3 and y_4), and silicon atoms are in the former T positions. As a result, the content of transition metal increases by a factor of two, while simultaneously the silicon content decreases by a factor of two. In the $TbFeSi_2$ structure the transition metal (Fe) is located in the 4*c* site with $y_4 \sim 0.75$ and silicon atoms are in the sites with $y_2 \sim 0.16$ and $y_3 \sim 0.04$. Depending on the X-ray scattering power of the atoms involved, such simple changes in the original structure $CeNiSi_2$ may result in noticeable differences for the XPD patterns. Fig. 6 illustrates how the distribution of the atoms in the unit cell changes the powder pattern intensities. For convenient comparison the patterns were calculated for ideal structures with identical atoms types and for identical orthorhombic unit cells ($0.425 \times 1.675 \times 0.417$ nm). For the tetragonal structure, however, the real values of the unit cell dimensions are used.

3.2. The crystal structures of $YbPd_2Si$ and $YbPt_2Si$

The crystal structures of $YbPd_2Si$ and $YbPt_2Si$ were both determined from single crystal X-ray data confirmed by XPD measurements. Both phases crystallize with the YPd_2Si-type (ordered version of Fe_3C). The crystallographic parameters for $YbPd_2Si$ and $YbPt_2Si$ are given in Table 4. According to XPD both phases $YbPd_2Si$ and $YbPt_2Si$ were obtained in single-phase condition (see Fig. 7).

The lattice parameters for the newly detected compounds $YbPd_2Si$ and $YbPt_2Si$ perfectly fit to the dependency of the unit cell parameters vs the rare earths in the series RPd_2Si and RPt_2Si earlier described by Moreau et al. [22]. As can be seen in Fig. 8 no anomalies are obvious for the cell dimensions and cell volumes for $YbPd_2Si$ and $YbPt_2Si$, therefore an Yb^{+3} ground state is inferred for the ytterbium atoms as recently reported for the low-temperature behavior of $YbPd_2Si$ [7].

Table 5
X-ray crystallographic data and structure refinement for $EuRh_{2+x}Si_{2-x}$ ($x=0.04$), $Sc_2Pt_3Si_2$ and $Eu_2Os_3Si_5$ standardized with program *Structure Tidy* [28].

Parameter	$EuRh_{2+x}Si_{2-x}$	$Sc_2Pt_3Si_2$	$Eu_2Os_3Si_5$
Alloy composition (at%)	$Eu_{25}Rh_{25}Si_{50}$	$Sc_{25}Pt_{50}Si_{25}$	$Eu_{25}Os_{25}Si_{50}$
Crystal size (μm)	$30\times30\times30$	$50\times40\times20$	$30\times30\times30$
Space group	*I*4/*mmm*, origin at inv. Centre	*Pbam*, origin at inv. centre	*P*4/*mnc*, origin at inv. centre
Prototype	$ThCr_2Si_2$	$Sc_2Pt_3Si_2$	$Sc_2Fe_3Si_5$
Pearson symbol	*tI*10	*oP*14	*tP*40
Lattice parameters (nm)[a]	$a=0.40920(2)$	$a=0.63488(2)$ $b=0.86803(2)$	$a=10.7276(2)$
	$c=1.02276$ (5)	$c=0.40324(2)$	$c=5.7615(1)$
Cell volume (nm^3)	0.171256(14)	0.222224(14)	0.66304(2)
Chemical formula	$EuRh_{2.035}Si_{1.965}$	$Sc_2Pt_3Si_2$	$Eu_2Os_3Si_5$
Formula weight, *M*	416.58	731.37	1014.97
Number of formula units in unit cell, *Z*	2	2	4
Calculated density (g/cm^3)	8.079	10.930	10.168
Absorption coefficient, μ_{abs} (mm^{-1})	28.18	97.33	76.71
2θ range up to (°)	65.73	72.60	72.53
Reflections in refinement	$113\leqslant4\sigma(F_o)$ of 121	$560\leqslant4\sigma(F_o)$ of 600	$849\leqslant4\sigma(F_0)$ of 867
Index range	$-6\leqslant h\leqslant6$ $-4\leqslant k\leqslant4$ $-15\leqslant l\leqslant15$	$-10\leqslant h\leqslant10$ $-14\leqslant k\leqslant14$ $-6\leqslant l\leqslant6$	$-17\leqslant h\leqslant17$ $-12\leqslant k\leqslant12$ $-9\leqslant l\leqslant8$
Number of variables	10	24	26
$R=\Sigma\|\|F_0\|-\|F_c\|\|/\Sigma\|F_0\|$	0.023	0.037	0.034
R_{Int}	0.017	0.022	0.023
wR_2	0.060	0.096	0.078
Goodness of fit, $S=\{\Sigma[w(F_o^2-F_c^2)^2]/(n-p)\}^{1/2}$	1.228	1.135	1.485
Extinction (Zachariasen)	0.017(2)	0.030(2)	0.0021(1)
Atom parameters			
Atom site 1	**2 Eu1** in 2*a* (0,0,0);	**4 Sc1** in 4*g* (*x*,*y*,0); $x=0.3910(2)$, $y=0.1698(2)$	**8 Eu1** in 8*h* (*x*,*y*,0); $x=0.26540(6)$, $y=0.42662(7)$
Occupation	1.00	1.00	1.00
$U_{eq.}$	0.0062(3)	0.0046(3)	0.0046(2)
Atom site 2	**4 Rh1** in 4*d* (0,1/2,1/4);	**4 Pt1** in 4*h* (*x*,*y*,1/2); $x=0.19141(4)$, $y=0.41333(3)$	**4 Os1** in 4*d* (0,1/2,1/4);
Occupation	1.00	1.00	1.00
$U_{eq.}$	0.0048(3)	0.0045(2)	0.0019(2)
Atom site 3	**4 Si1/Rh** in 4*e* (0,0,*z*); $z=0.3708(2)$	**2 Pt2** in 2*a* (0,0,0);	**8 Os2** in 8*h* (*x*,*y*,0); $x=0.14739(5)$, $y=0.12602(5)$
Occupation	0.98(1) Si +0.02 Rh	1.00	1.00
$U_{eq.}$	0.0072(8)	0.0039(2)	0.0030(1)
Atom site 4		**4 Si1** in 4*h* (*x*,*y*,1/2); $x=0.0753(4)$, $y=0.1501(3)$	**4 Si1** in 4*e* (0,0,*z*); $z=0.2378(10)$
Occupation		1.00	1.00
$U_{eq.}$		0.0047(4)	$U_{iso}=0.0034(9)$
Atom site 5			**8 Si2** in 8*h* (*x*,*y*,0); $X=0.0251(4)$, $y=0.3203(4)$
Occupation			1.00
$U_{eq.}$			$U_{iso}=0.0017(6)$
Atom site 6			**8 Si3** in 16*i* (*x*,*y*,*z*); $x=0.3352(5)$, $y=0.1805(5)$, $z=0.2239(11)$
Occupation			0.50
$U_{eq.}$			$U_{iso}=0.0037(9)$,

Residual density; e/Å^3 max; min		3.90		−1.68		9.14		−8.31		5.89		−4.58
Interatomic distances, nm, (eds < 0.0007 nm)	Eu1-	8 Si1	Sc1-	0.3181	Pt1-	2 Si1	Eu1-	0.2807	Eu1-	1 Si2		0.2819
		8 Rh1		0.3275		2 Si1		0.2848		2 Si3		0.3003
	Rh1-	4 Si1		0.2390		2 Pt1		0.2868		2 Si3		0.3033
		4 Rh1		0.2894		1 Pt2		0.2887		2 Si1		0.3039
		4 Eu1		0.3275		1 Pt2		0.2948		2 Si21		0.3068
	Si1-	4 Rh1		0.2390		2 Pt1		0.3049		2 Os2		0.3207
		1 Si1		0.2643		2 Pt1	Os1-	0.3184		4 Si2		0.2421
		4 Eu1		0.3181		1 Sc1		0.3257		4 Si3		0.2626
						2 Sc1		0.3466		2 Os1		0.2881
					Pt1-	1 Si1	Os2-	0.2401		2 Si3		0.2463
						1 Si1		0.2499		1 Si2		0.2463
						1 Si1		0.2533		1 Si2		0.2463
						1 Pt1		0.2859		2 Si3		0.2473
						2 Sc1		0.2868		2 Si1		0.2491
						2 Pt2		0.2910	Si1-	4 Os2		0.2491
						2 Sc1		0.3049		1 Si1		0.2740
						2 Sc1		0.3184		4 Eu1		0.3039
					Pt2-	4 Si1		0.2448	Si2-	2 Os1		0.2421
						2 Sc1		0.2887		1 Os2		0.2463
						4 Pt1		0.2910		1 Os2		0.2463
						2 Sc1		0.2948		2 Si3		0.2560
					Si1-	1 Pt1		0.2401		1 Eu1		0.2819
						2 Pt2		0.2448	Si3-	1 Os2		0.2463
						1 Pt1		0.2499		1 Os2		0.2473
						1 Pt1		0.2533		1 Si2		0.2560
						1 Si1		0.2776		1 Si3		0.2579
						2 Sc1		0.2807		1 Si2		0.2584
						2 Sc1		0.2848		1 Os1		0.2626
										1 Eu1		0.3003
										1 Eu1		0.3033

3.3. The crystal structures of $Eu_2Os_3Si_5$, $Sc_2Pt_3Si_2$ and $EuRh_2Si_2$

While searching for new compounds with stoichiometrics 1:1:2 and 1:2:1 single crystals of good quality were found for two new compounds, $Eu_2Os_3Si_5$, $Sc_2Pt_3Si_2$, as well as for $EuRh_2Si_2$, which was characterized earlier from powder data [29–31]. Results of the X-ray crystal refinements are presented in Table 5.

3.3.1. $Eu_2Os_3Si_5$

A single crystal, separated from the as-cast alloy $Eu_{25}Os_{25}Si_{50}$ (nominal composition in at%) revealed a tetragonal unit cell (a=1.07276(2) nm, c=0.57615(7) nm) and extinctions $0kl$: (k+l=$2n$+1), hhl (l=$2n$+1), $00l$ (l=$2n$+1) and $h00$ (h=$2n$+1) consistent with space groups $P4nc$ (No. 104) and $P4/mnc$ (No. 128). Refinement of the structure in non-centrosymmetric $P4nc$ (No. 104) space group resulted in Flack parameter value 0.5(2) and worse atomic displacement parameters, so we choose space group $P4/mnc$ (No. 128). Direct methods yielded an atomic arrangement isotypic with the structure type of $Sc_2Fe_3Si_5$ [39]. Anisotropic atomic displacement parameters yielded an elongated ellipsoid for the Si atoms in 8g, which in the following was split (Fig. 9). Results of the refinement for $Eu_2Os_3Si_5$, which converged to R=0.034 with residual electron densities smaller than $\pm 5.9\,e^-/Å^3$, are summarized in Table 5.

The $Sc_2Fe_3Si_5$-type structure was discussed by Chabot and Parthe [40] as an intergrowth of structural slabs of the $CaBe_2Ge_2$ structure and a second slab related to the $BaNiSn_3$ structure. Analyzing literature data for $R_2T_3Si_5$ compounds we found than in a few cases the 8g site (Si in x, x+1/2, 1/4) also revealed either enhanced values for U_{iso} or elongated thermal ellipsoids. For example in $Sm_2(Ru_{1.72}Os_{1.28})Si_5$ displacement of the Si atoms in 8g site reaches with $U_{eq.}\times 100$=1.39 (23) Å^2 a maximum value in the structure [41] and for stoichiometric $Sm_2Ru_3Si_5$ atom displacement of the Si atoms showed a long ellipsoid: U_{11}=0.019(1), U_{22}=0.019(1), U_{33}=0.0418(26), U_{12}=0.0077(14), U_{13}=0.0174(13), U_{23}=0.0174(13) [42]. The splitting of the silicon site for $Eu_2Os_3Si_5$ from 8g into 16i with occupancy 0.5 resolved the problem with the ADP parameter. The interatomic distances in $Eu_2Os_3Si_5$ are in the range usually observed for intermetallic compounds (Table 5).

3.3.2. $Sc_2Pt_3Si_2$

A single crystal, broken from an as-cast alloy with composition $Sc_{25}Pt_{50}Si_{25}$ (at%), revealed orthorhombic symmetry with space group $Pbam$ and lattice parameters: a=0.63488(2) nm, b=0.86803(2) nm, c=0.40324(2) nm) (Z=2). The structure was solved by direct methods yielding a fully ordered distribution of Sc, Pt and Si atoms. Results of the refinement, which converged to R=0.037 are summarized in Table 5. Scandium atoms are located in pentagonal prisms with five additional atoms (2 Pt and 3 Sc, coordination number CN=15). Each Pt1 atom is surrounded by 12 atoms (6 Sc1, 2 Pt2, 1 Pt1, 3 Si1) forming a distorted tetragonal prism with four additional atoms centering the lateral faces (CN=12). Pt2 atoms are located in quadrangular prisms with four additional Sc atoms (CN=12). Silicon atoms are located in quadrangular antiprisms (4 Sc+4 Pt) capped by two additional (Pt1+Si) atoms (CN=10). A perspective vision of the $Sc_2Pt_3Si_2$ crystal structure with the coordination polyhedra is shown in Fig. 10.

$Sc_2Pt_3Si_2$ represents a new structure type, which can be described as a packing of triangular and quadrangular prisms around the Si1 and the Pt1 atoms, respectively (Fig. 11). XPD patterns of $Sc_{25}Pt_{50}Si_{25}$ and $Sc_{28.6}Pt_{42.8}Si_{28.6}$ (2:3:2) alloys reveal the $Sc_2Pt_3Si_2$ phase to be a secondary phase in both as-cast and

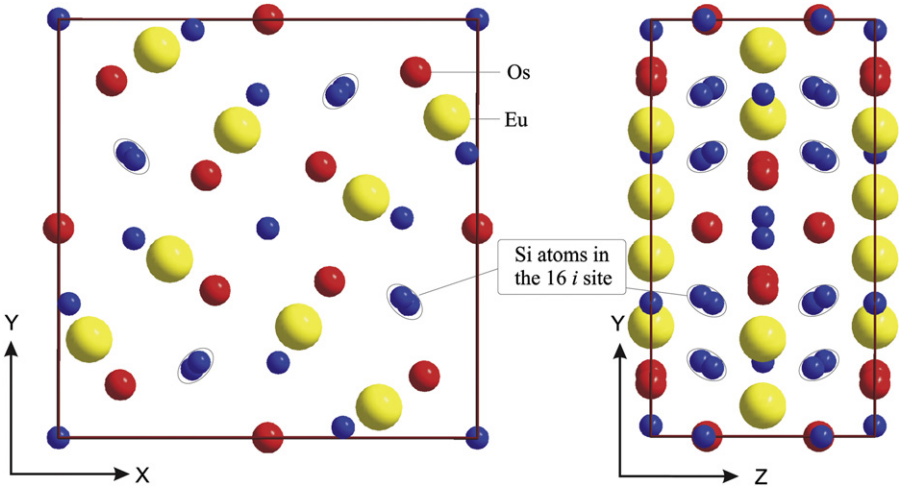

Fig. 9. Projections of the $Eu_2Os_3Si_5$ crystal structure on the planes *XY* and *YZ*.

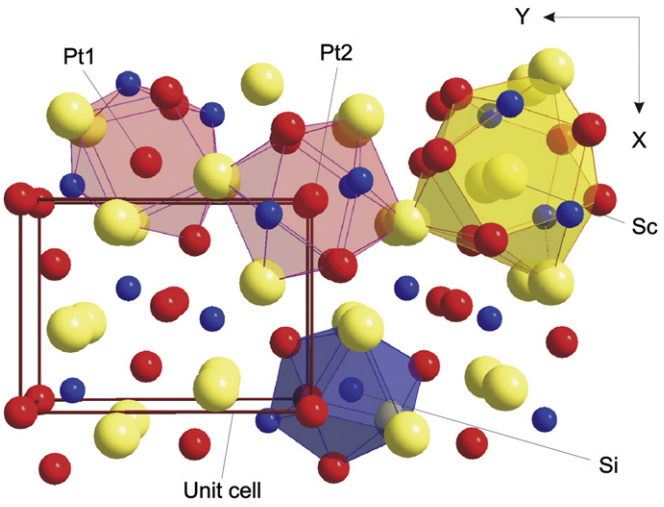

Fig. 10. The crystal structure of $Sc_2Pt_3Si_2$ in perspective view along [001] and coordination polyhedra of the atoms.

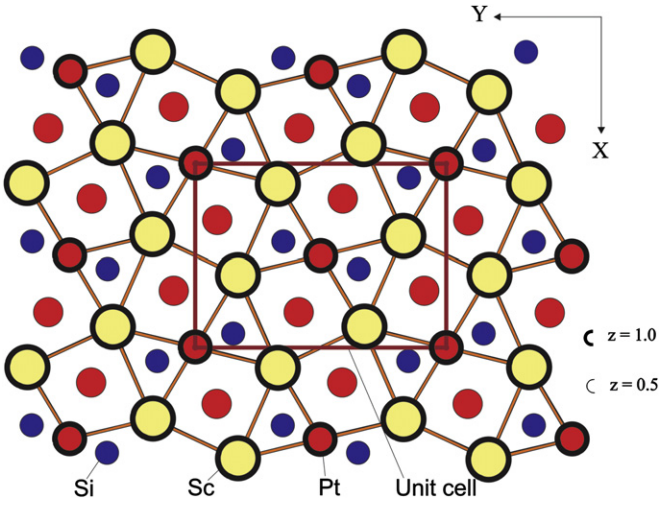

Fig. 11. The crystal structure of $Sc_2Pt_3Si_2$ as a packing of triangular and quadrangular prisms projected on the *XY* plane.

annealed specimens. Moreover, the amount of $Sc_2Pt_3Si_2$ in the alloy $Sc_{28.6}Pt_{42.8}Si_{28.6}$ (2:3:2) noticeably decreased after annealing at 900 °C, so one can suppose this phase to be a high-temperature phase. The interatomic distances in the $Sc_2Pt_3Si_2$ crystal structure are characterized by values typical for intermetallics (Table 5).

3.3.3. $EuRh_2Si_2$

The crystal structure of the $EuRh_2Si_2$ was re-determined on a single crystal taken from the surface of the as-cast alloy $Eu_{25}Rh_{25}Si_{50}$. $EuRh_2Si_2$ crystallizes in the tetragonal $ThCr_2Si_2$-type (space group $I4/mmm$, $Z=2$, lattice parameters $a=0.40920(2)$ nm, $c=1.02276(5)$ nm). The structure was refined with anisotropic atomic displacement parameters for all atoms down to $R=0.023$ with residual electron densities less than $\pm 3.9\,e^-/Å^3$. A statistical occupation of the 4*e* site by (0.98 Si +0.02 Rh) atoms was detected. The structure parameters are presented in Table 5. The result obtained in the present work confirmed the powder XRD data for $EuRh_2Si_2$ previously reported in the literature [29–31].

4. Conclusion

The unique crystal structure of the compounds $CeIr_2Si$, $LaRh_2Si$ and $LaIr_2Si$ was determined for the first time and can be presented as a packing of AlB_2- and $BaAl_4$-slabs. The $CeIr_2Si$-type is related to the $CeNiSi_2$-type. Other new representatives of this structural family, $EuPt_{1+x}Si_{2-x}$ ($CeNiSi_2$-type), $EuPt_2Si$ (inverse $CeNiSi_2$-type) and four Ag-containing silicides $LaAgSi_2$, $CeAgSi_2$, $PrAgSi_2$ and $NdAgSi_2$ (all of the $TbFeSi_2$-type), were synthesized and studied by X-ray diffraction technique. The simple relations between orthorhombic $CeNiSi_2$-type, inverse $CeNiSi_2$-type and $TbFeSi_2$-type and their relationship with the new tetragonal $CeIr_2Si$-type were illustrated along with the corresponding XPD patterns. X-ray single crystal CCD data of $YbPd_2Si$ and $YbPt_2Si$ revealed isotypism with the YPd_2Si-type (ordered version of Fe_3C). No $RT_2Si/RTSi_2$ compounds were detected in the $Sc_{25}Pt_{50}Si_{25}$, $Eu_{25}Os_{25}Si_{50}$ and $Eu_{25}Rh_{25}Si_{50}$ alloys in which, however, the new compounds $Sc_2Pt_3Si_2$ (own type) and $Eu_2Os_3Si_5$ ($Sc_2Fe_3Si_5$-type) as well as $EuRh_2Si_2$ ($ThCr_2Si_2$-type) were detected and studied from X-ray single crystal data.

Acknowledgments

This research was supported by the Austrian National Science Foundation FWF Project P18054-Phy. The authors are grateful to the Russian Foundation of Basic Research for support of the Project No. 08-03-01072 and to the bilateral WTZ Austria–Russia, Project 17/2006.

Appendix A. Supplementary material

Supplementary data associated with this article can be found in the online version at doi:10.1016/j.jssc.2010.03.038.

References

[1] E. Bauer, G. Hilscher, H. Michor, C. Paul, E.W. Scheidt, A.V. Gribanov, Y.D. Seropegin, H. Noël, M. Sigrist, P. Rogl, Phys. Rev. Lett. 92 (2004) 027003/1–027003/4.
[2] N. Kimura, K. Ito, K. Saitoh, Y. Umeda, H. Aoki, T. Terashima, Phys. Rev. Lett. 95 (2005) 247004/1–247004/4.
[3] I. Sugitani, Y. Okuda, H. Shishido, T. Yamada, A. Thamizhavel, E. Yamamoto, T.D. Matsuda, Y. Haga, T. Takeuchi, R. Settai, Y. Onuki, J. Phys. Soc. Japan 75 (2006) 043703-1–043703-4.
[4] J.M. Barandiaran, D. Gignoux, D. Schmitt, J.C. Gomez-Sal, Solid State Commun. 59 (1986) 223–225.
[5] E. Bauer, G. Hilscher, H. Kaldarar, H. Michor, E.W. Scheidt, P. Rogl, A. Gribanov, Y. Seropegin, J. Magn. Magn. Mater. 310 (2007) e73–e75.
[6] Y. Muro, S. Takahashi, K. Sunahara, K. Motoya, M. Akatsu, N. Shirakawa, J. Magn. Magn. Mater. 310 (2007) e40–e41.
[7] E. Bauer, H. Kaldarar, H. Michor, M. Reissner, E. Royanian, E.W. Scheidt, P. Rogl, A. Gribanov, Y. Seropegin, Phys. B: Condens. Matter 403 (2008) 919–921.
[8] W.H. Lee, K.S. Kwan, P. Klavins, R.N. Shelton, Phys. Rev. B 42 (1990) 6542–6545.
[9] B. Chevalier, P. Rogl, K. Hiebl, J. Etourneau, J. Solid State Chem. 107 (1993) 327–331.
[10] V.N. Duginov, V.G. Grebinnik, K.I. Gritsaj, T.N. Mamedov, V.G. Olshevsky, V.Y. Pomjakushin, V.A. Zhukov, I.A. Krivosheev, A.N. Ponomarev, V.N. Nikiforov, Y.D. Seropegin, M. Baran, H. Szymczak, Phys. Rev. B: Condens. Matter Mater. Phys. 55 (1997) 12343–12347.
[11] V.K. Pecharsky, K.A. Gschneidner Jr., L.L. Miller, Phys. Rev. B 43 (1991) 10906–10914.
[12] D.T. Adroja, B.D. Rainford, Phys. B: Condens. Matter 230–232 (1997) 762–765.
[13] J.J. Lu, C. Tien, L.Y. Jang, C.S. Wur, Phys. B: Condens. Matter 305 (2001) 105–112.
[14] O.I. Bodak, E.I. Gladyshevskii, Sov. Phys. Crystallogr. 14 (1970) 859–862.
[15] V.I. Yarovetz, Y.K. Gorelenko, Vestn. L'vovsk. Univ., Ser. Khim. 43 (1981) 20–23 (in Russian).
[16] L. Paccard, D. Paccard, J. Allemand, J. Less-Common Met. 161 (1990) 295–298.
[17] M. Francois, G. Venturini, E. McRae, B. Malaman, B. Roques, J. Less-Common Met. 128 (1987) 249–257.
[18] K. Cenzual, R.E. Gladyshevskii, E. Parthe, Acta Crystallogr. C 48 (1992) 225–228.
[19] R. Welter, G. Venturini, B. Malaman, J. Alloys Compd. 185 (1992) 235–240.
[20] L.S. Andrukhin, L.A. Lysenko, Y.P. Yarmolyuk, E.I. Gladyshevskii, Dopov. Akad. Nauk Ukr. RSR, Ser. A (1975) 645.
[21] J. Steinmetz, G. Venturini, B. Roques, N. Engel, I. Chabot, E. Parthe, Acta Crystallogr. B 38 (1982) 2103–2108.
[22] J.M. Moreau, J.L. Roy, D. Paccard, Acta Crystallogr. B 38 (1982) 2446–2448.
[23] STOE WINXPOW (Version 1.06), Stoe & Cie GmbH, Darmstadt, Germany, 1999.
[24] J. Rodriguez-Carvajal, Physica B 192 (1993) 55–69.
[25] T. Roisnel, J. Rodriguez-Carvajal, Materials science forum, in: Proceedings of the European Powder Diffraction Conference (EPDIC7), 2000, p. 118.
[26] Nonius Kappa CCD Program Package COLLECT, DENZO, SCALEPACK, SORTAV, Delft, Nonius, The Netherlands, 1998.
[27] G.M. Sheldrick, Acta Crystallogr. A 64 (2008) 112–122.
[28] E. Parthe, L. Gelato, B. Chabot, M. Penzo, K. Cenzual, R. Gladyshevskii, TYPIX Standardized Data and Crystal Chemical Characterization of Inorganic Structure Types, Springer-Verlag, Berlin, Heidelberg, 1994.
[29] I. Felner, I. Nowik, J. Phys. Chem. Solid 45 (1984) 419–426.
[30] B. Chevalier, J.M.D. Coey, B. Lloret, J. Etourneau, J. Phys. C: Solid State Phys. 19 (1986) 4521–4528.
[31] Z. Hossain, O. Trovarelli, C. Geibel, F. Steglich, J. Alloys Compd. 323–324 (2001) 396–399.
[32] A.I. Tursina, A.V. Gribanov, Y.D. Seropegin, A.A. Novitskii, O.I. Bodak, J. Alloys Compd. 367 (2004) 146–148.
[33] A. Lipatov, A. Gribanov, A. Grytsiv, S. Safronov, P. Rogl, J. Rousnyak, Y. Seropegin, G. Giester, J. Solid State Chem. 183 (2010) 829–843.
[34] O.V. Zaplatynsky, Y.M. Prots, P.S. Salamakha, L.O. Muratova, O.I. Bodak, J. Alloys Compd. 232 (1996) L1–L4.
[35] O. Bardin, O. Bodak, O. Protsyk, Z. Shpyrka, Visnyk Lviv. Univ., Ser. Khim. 40 (2001) 57–60.
[36] B. Belan, O. Bodak, R. Gladyshevskii, I. Soroka, B. Kuzhel, O. Protsyk, I. Stets, J. Alloys Compd. 396 (2005) 212–216.
[37] I.A. Savysyuk, Phase equilibria, crystal structures and electrical properties of compounds in the systems {Y,Pr}–Ag–{Si,Ge,Sn}, Ph.D. Thesis, University of Lviv, 2001.
[38] E. Cordruwisch, D. Kaczorowski, P. Rogl, A. Saccone, R. Ferro, J. Alloys Compd. 320 (2001) 308–319.
[39] Ya.P. Yarmoluyk, L.G. Aksel'rud, E.I. Gladyshevskii, Sov. Phys. Crystallogr. (Engl. Transl.) 22 (1977) 358.
[40] B. Chabot, E. Parthe, J. Less-Common Met. 97 (1984) 285–290.
[41] C. Rizzoli, O.L. Sologub, P.S. Salamakha, J. Alloys Compd. 337 (2002) L4–L7.
[42] P. Salamakha, O. Sologub, G. Bocelli, L. Righi, J. Alloys Compd. 299 (2000) L6–L8.
[43] O.L. Borisenko, O.I. Bodak, Y.D. Seropegin, V.N. Nikiforov, M.V. Kovachikova, Y.V. Kochetkov, Izv. Akad. Nauk SSSR. Metally 2 (199) 167–172 (in Russian).
[44] B. Chevalier, P. Lejay, J. Etourneau, P. Hagenmuller, Mater. Res. Bull. 18 (1983) 315–330.
[45] D.T. Adroja, B.D. Rainford, J. Magn. Magn. Mater. 119 (1993) 54–58.
[46] J.J. Lu, M.K. Lee, Y.M. Lu, L.Y. Jang, J. Magn. Magn. Mater. 311 (2007) 614–617.
[47] J.J. Lu, C. Tien, L.Y. Jang, Solid State Commun. 120 (2001) 29–33.